Heat Transport without Heating?-An Ultrafast X-Ray Perspective into a Metal Heterostructure

Jan-Etienne Pudell, Maximilian Mattern, Michel Hehn, Grégory Malinowski, Marc M Herzog, Matias Bargheer

ADVANCED FUNCTIONAL MATERIALS
www.afm-journal.de

Heat Transport without Heating?—An Ultrafast X-Ray Perspective into a Metal Heterostructure

*Jan-Etienne Pudell, Maximilian Mattern, Michel Hehn, Grégory Malinowski, Marc Herzog, and Matias Bargheer**

When the spatial dimensions of metallic heterostructures shrink below the mean free path of its conduction electrons, the transport of electrons and hence the transport of thermal energy by electrons continuously changes from diffusive to ballistic. Electron–phonon coupling sets the mean free path to the nanoscale and the time for equilibration of electron and lattice temperatures to the picosecond range. A particularly intriguing situation occurs in trilayer heterostructures combining metals with very different electron–phonon coupling strength: Heat energy deposited in few atomic layers of Pt is transported into a nanometric Ni film, which is heated more than the Cu film through which the heat is released. Femtosecond pump-probe experiments with hard X-ray pulses provide a layer-specific probe of the heat energy. A purely diffusive two-temperature model with increased thermal conductivity of hot electrons excellently reproduces the observed signals from all three layers. At the time when the Ni lattice is maximally heated, no significant heat has entered the Cu lattice. This phenomenon would be enhanced in thinner layers where ballistic transport dominates. In this context it is shown that purely diffusive transport can lead to a linear time-to-length dependence that must not be misinterpreted as ballistic transport.

1. Introduction

In macroscopic engineering contexts, heat transport in metals is well described by the heat equation using macroscopic thermophysical parameters of the constituent materials and additional interface thermal resistances.[1,2] This differential equation is analogous to the diffusion of quasiparticles carrying heat.[3] In metals both conduction electrons and phonons contribute, and the non-equilibrium between these two subsystems has to be taken into account at short time and length scales. Ab-initio modeling of this complex problem is an active field of theoretical physics.[4–7] While the electrons rapidly acquire a Fermi-distribution, the temperature of the lattice may not be a well defined quantity for hundreds of picoseconds.[8] The non-thermal occupation of phonon modes can be described by mode-specific temperatures.[5] When the length scale of the system falls below the mean free path of the heat carrying quasiparticles, a superdiffusive and finally ballistic regime of energy transport is reached as the number of scattering events per quasiparticle approaches zero (cf. **Figure 1**a).[9–11] For timescales beyond the thermalization of the electron system, which is typically much faster than electron-phonon (e-ph) coupling, thermal transport within each subsystem can be approximated within a diffusive two-temperature model (TTM). Remarkably, if electrons injected into a metal layer from one side traverse it ballistically at the Fermi velocity, the electronic energy is transported through the layer without heating it. In a superdiffusive regime only a small part of the electron energy dissipated by few scattering events remains in the layer. In magnetic metals, the spin degree of freedom not just complicates the problem by offering additional scattering channels.[9] The controlled manipulation of spins by hot electrons or lattice strain is a growing field of active research as it may revolutionize data processing and storage.[12–16] Superdiffusive electrons excited by femtosecond light pulses have been shown to lead to demagnetization, spin precession, and magnetization switching both in experiment and theory.[9,17–19] Electronically controlled heat pulses highlighted the potential for embedding these phenomena in modern CMOS technology.[20,21] Time-domain thermoreflectance is becoming an increasingly useful tool in material science for determining thermal conductivities of the constituents and interfaces in heterostructures.[2] However, for metal layers thinner than their skin depth the analysis is complicated. The optical response mixes contributions of adjacent layers. Thus, layers sandwiched between two metals cannot be independently analyzed. Femtosecond pump-probe experiments using X-rays can yield important additional insights, particularly when probing specific subsystems containing the heat energy.[22–27] Recently, ultrafast X-ray diffraction (UXRD) experiments revealed the unconventional heat transport in a bilayer of 5 nm Au and 10 nm Ni. It does not matter

J.-E. Pudell, M. Mattern, Dr. M. Herzog, Prof. M. Bargheer
Institut für Physik & Astronomie
Universität Potsdam
Karl-Liebknecht-Str. 24-25, 14476 Potsdam, Germany
E-mail: bargheer@uni-potsdam.de
J.-E. Pudell, Prof. M. Bargheer
Helmholtz-Zentrum Berlin für Materialien und Energie GmbH
Wilhelm-Conrad-Röntgen Campus, BESSY II, 12489 Berlin, Germany
Prof. M. Hehn, Dr. G. Malinowski
Institut Jean Lamour (UMR CNRS 7198)
Université Lorraine
2 allée André Guinier, Campus Artem, Nancy 54000, France
The ORCID identification number(s) for the author(s) of this article can be found under https://doi.org/10.1002/adfm.202004555.

DOI: 10.1002/adfm.202004555

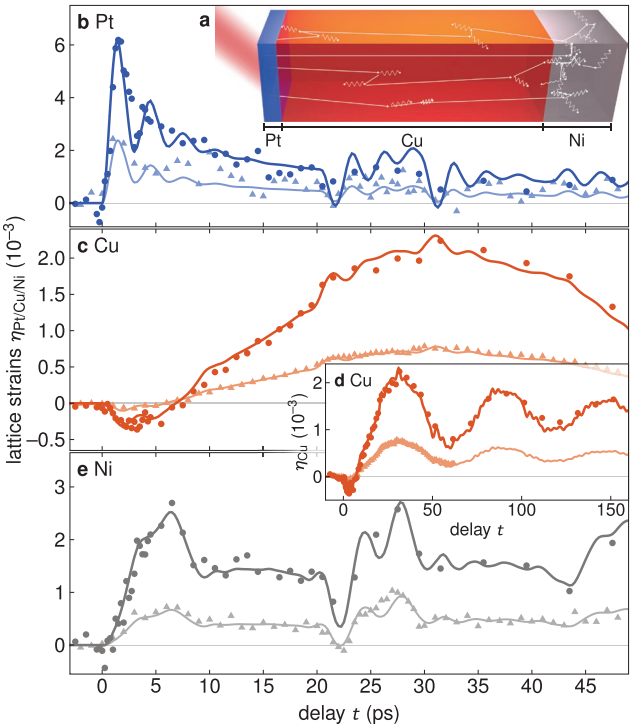

Figure 1. Layer specific UXRD data. a) Sketch of the heat transport from the exited Pt layer (blue) by electrons through a Cu layer (orange) to a Ni layer (gray). b–e) Transient lattice strains $\eta_{Pt/Cu/Ni}$ for two different excitation fluences (6.5 mJ cm^{-2} [faint colors] and 20 mJ cm^{-2} [bright colors]) of Pt, Cu, and Ni, respectively. The continuous lines originate from a simulation considering diffusion according to a TTM with the temperature-dependent electron heat conductivity according to Equation (2).

if the optical absorption occurs in Au or Ni—the electronic heat energy is very rapidly ($\lesssim$1 ps) captured by the electrons and phonons in Ni, whereas the Au lattice heats up surprisingly slowly on a 100 ps timescale. This observation can be rationalized by a modified TTM.[25]

Here we show that electronic heat energy deposited in a 6 nm Pt film is very rapidly transported by hot electrons through a 100 nm thick Cu layer without significantly heating it. The electronic heat energy is rapidly extracted by a 20 nm thick Ni layer at the backside of the Cu layer, because Ni offers a large electronic heat capacity, which is proportional to the electronic density of states at the Fermi level.[28] Rapid e-ph coupling in Ni cools down the Ni electrons, preserving a large temperature gradient between the electron systems in Cu and Ni. We experimentally confirm this model by measuring the lattice expansion of Pt, Cu, and Ni by UXRD with sub-picosecond time resolution in a laser-based laboratory setup. Directly after laser pulse excitation of the Pt layer, the buried Ni layer shows a very rapid expansion, whereas the Cu layer is initially compressed before it slowly expands. A fully diffusive TTM of the coupled phonon and electron heat transport excellently reproduces the data simultaneously for all three layers and for several excitation conditions with one set of parameters. The model shows that the Ni lattice is heated by hot electrons much faster and to higher temperatures than the Cu lattice. Although our modeling clearly simplifies the analysis by neglecting ballistic or superdiffusive transport and non-thermal distributions in the phonon system,[5,6] the observed phenomenon of counter-intuitive heating of the back-end of the heterostructure is described correctly. In fact, it is underestimated, since ballistic or superdiffusive motion of electrons would even increase the heating of the distant Ni layer.

Moreover, the conceptually simple diffusive modeling made us aware of a potential pitfall in deducing the transport mechanism in photoexcited metal layers from pump-probe experiments: Our model surprisingly predicts that the rise time $\tau_{10\%}$ of the Ni electron temperature to the 10% level of its maximum temperature change depends linearly on the Cu layer thickness d. Given the exclusively diffusive character of our model, our finding implies that an interpretation of similar experimental signatures as a manifestation of ballistic transport may be illegitimate. In contrast, the rise time by an absolute temperature change ΔT of the Ni layer shows the dependence $\tau_{\Delta T} \propto d^2$, which is characteristic of diffusion.

2. UXRD Experiment

We excite a metal heterostructure with a femtosecond laser pulse which is essentially absorbed in the 6 nm thick Pt cap layer (see experimental section). Figure 1 shows the transient average lattice strain of Pt (Figure 1b), Cu (Figure 1c,d) and Ni (Figure 1e) measured by UXRD for two different excitation fluences. The Pt layer expands immediately after the optical excitation. The maximum expansion is observed at t = 1.5 ps, as expected from the propagation of the expansion wave through the Pt layer at the sound velocity v_{Pt}.[29] The pronounced minimum at t = 3 ps indicates the back-reflection of the expansion wave at the sample surface leading to a strongly damped oscillation of the Pt layer thickness with period T_{Pt} = 3 ps. Within 25 ps the Pt strain decreases to a nearly constant level of $\eta_{Pt} = 1 \cdot 10^{-3}$ by thermal transport to the Ni and Cu layer. Surprisingly, it is the buried Ni layer that expands right after the Pt, reaching a maximum expansion around 6 ps. The asymmetry of the maximum is due to the reflection of the Ni expansion wave at the interfaces of the Ta buffer layer and the glass substrate (see Section 3 for a thorough modeling). The Ni signal modulation in the 20–30 ps range is caused by the pronounced acoustic strain pulse launched by the Pt layer and its reflections. Thermal expansion of the Cu layer, through which the heat was conducted to the Ni layer, occurs later and triggers a Cu thickness oscillation with 60 ps period, which results from acoustic reflections at the sample surface and the glass interface.

The delayed slow heating of the Cu layer is directly evidenced by the initial compression of Cu prevailing for more than 5 ps (Figure 1c). Only the first t = 3 ps can be explained by the compressive leading part of the bipolar strain wave launched by the Pt expansion. After this time, even the expansive part of this bipolar strain pulse has completely entered the Cu layer.[26,27] The additional prolonged compression of Cu must originate from the leading part of a bipolar strain wave generated in the buried Ni layer that is almost four times thicker than the Pt. The combined experimental data of Figure 1 directly show that the Ni layer expands much faster and stronger than the Cu layer, through which the heat is conducted toward the Ni layer in the first place.

3. Modeling

In the previous section we have implicitly used the lattice expansion as a layer-specific thermometer. Indeed, the thermal strain $\eta \propto \sigma$ is proportional to the driving stress $\sigma = \Gamma\rho^{Q}$, which is in turn proportional to the energy density ρ^{Q}. Here, Γ is the macroscopic Grüneisen constant. In metals, at least two contributions to the stress must be distinguished, namely, electrons and phonons. At room temperature the specific heat of the phonons C_{ph} is nearly constant in the Dulong-Petit limit. Therefore, the change of the phonon energy density $\Delta\rho^{Q}_{ph} = C_{ph}\Delta T_{ph}$ due to the laser excitation is proportional to the phonon temperature rise ΔT_{ph}. This makes our X-ray thermometer simple to read at timescales beyond 1 ps, when the energy in the electron system can be neglected. In this limit, the measured strain is directly proportional to the phonon temperature rise, $\eta \propto \Delta T_{ph}$. In contrast, the energy density change in the electron system $\Delta\rho^{Q}_{e} = C_e(T_e)\Delta T_e$ has a quadratic contribution in ΔT_e due to the Sommerfeld model of the electronic heat capacity $C_e(T_e) = \gamma^{S}(T_e^0 + \Delta T_e)$ where γ^{S} is the Sommerfeld constant and T_e^0 is the starting temperature. The electronic stress contribution $\sigma_e = \Gamma_e\rho^{Q}_{e}$ is only present in the first picosecond, but it strongly influences the shape and size of the strain waves.

The timings of the three measured strain transients in Figure 1 already indicate that Ni heats up strongly before Cu even gets warm. In the following we lay out a more quantitative analysis using a diffusive 1D TTM.[30] The model describes the evolution of the electron and lattice temperatures due to diffusion and mutual coupling using the classical TTM:

$$\begin{aligned} C_e(T_e)\frac{\partial T_e}{\partial t} &= \frac{\partial}{\partial z}\left(\kappa_e(T_e, T_{ph})\frac{\partial T_e}{\partial z}\right) + g(T_{ph} - T_e) + S_e(z,t) \\ C_{ph}\frac{\partial T_{ph}}{\partial t} &= \frac{\partial}{\partial z}\left(\kappa_{ph}\frac{\partial T_{ph}}{\partial z}\right) + g(T_e - T_{ph}) \end{aligned} \quad (1)$$

The laser pulse heats the electrons via the source term $S_e(z, t)$, $\kappa_{e/ph}$ are the electron and phonon thermal conductivities, respectively, and g is the e-ph coupling parameter. The spatial coordinate z is directed perpendicular to the sample surface.

The phonons contribute to heat transport; however, already in thermal equilibrium the electron heat conductivity dominates by far.[28] For a correct description of the non-equilibrium transport, it is vital to include the dependence of the electron heat conductivity κ_e on the phonon and electron temperatures.[31–34] In the relevant temperature range the electronic specific heat can be approximated by $C_e = \gamma^{S}T_e$ and the mean scattering time of the electrons $\tau_e \propto 1/T_{ph}$ is dominated by e-ph scattering.[31–34] For the conduction band electrons of Cu, kinetic gas theory yields

$$\kappa_e(T_e, T_{ph}) = \frac{1}{3}C_e v_F \bar{l} = \frac{1}{3}C_e v_F^2 \tau_e = \kappa_e^0 \frac{T_e}{T_{ph}} \quad (2)$$

The empirical equilibrium conductivity κ_e^0 encodes γ^{S}, the Fermi velocity v_F and the proportionality constant in $\tau_e \propto 1/T_{ph}$. The mean free path $\bar{l} = v_F\tau_e$ is independent of T_e and only depends on T_{ph}. This text-book model was recently applied to model the in-plane heat transport in a nanometric metal film.[35]

Table 1. Thermophysical parameters of Pt, Cu, Ni, Ta, and the glass substrate taken from the indicated literature. Values in brackets are optimized values for the simulation.

	Pt	Cu	Ni	Ta	Glass
γ^{S} (mJ cm^{-3} K^{-2})	0.74[33]	0.10[33]	1.06[33]	0.38[51]	–
C_{ph} (J cm^{-3} K^{-1})	2.85[52]	3.44	3.94	2.33[51]	1.80[53]
κ_e^0 (W m^{-1} K^{-1})	66[54]	396[33]	81[33,55]	52	–
κ_{ph} (W m^{-1} K^{-1})	5[54]	5	9.6[55]	5	1[53]
g (PW m^{-3} K^{-1})	400[56]	63[56]	360[56]	100	–
ρ (g cm^{-3})	21.45	8.96	8.91	16.68	2.54[53]
ν_s (nm^{-1} ps)	4.2[57,58]	5.2[56,90]	6.3[61]	4.2	5.7[53]
Γ_e	2.4[62] (0.9)	0.9[62] (1.1)	2.0[62]	1.3[62]	–
Γ_{ph}	3.0[62] (2.5)	1.7[62] (2.1)	1.65[62]	1.5[62]	0.3[53]

The thermophysical parameters used in our modeling are listed in **Table 1**. For an incident excitation fluence of 20 mJ cm^{-2} we obtain the spatio-temporal temperature maps $T_{e/ph}(z, t)$ of the electron and phonon systems shown in **Figure 2**. For convenience, the heterostructure is shown at the top of Figure 2. We find that the hot electrons (Figure 2a) very rapidly (few 100 fs) diffuse from the Pt through the Cu into the Ni layer. Due to the strong e-ph coupling in Ni, the electron energy is rapidly dissipated to the Ni lattice, thus preserving a large temperature gradient between the electron systems in Cu and Ni. The electron temperature equilibrates throughout the heterostructure within 1.4 ps. Figure 2c emphasizes the decisive role of the large electronic heat capacity of Pt and Ni, which originates from the large electronic density of states at the Fermi level. The Ni layer is buried far beyond the skin depth of the metal heterostructure and can only be heated by transport through Cu. Figure 2b reveals that the lattice temperature of the Ni layer rises within 1–2 ps. The Pt lattice gets heated on a similar timescale to even higher temperatures, because the Pt layer directly absorbs the photon energy. The rapid diffusion of hot electrons competes with the strong e-ph coupling in Pt. The energy density of the phonons in Figure 2d is nearly identical to the temperature map in Figure 2b since the lattice heat capacity is constant close to the Dulong-Petit limit. Note that the existence of interfaces between different metals may give rise to thermal interface resistance. The fact that we do not need to take interface resistances into account in order to obtain agreement between experiment and calculations suggests that such interface effects are negligible here.

After e-ph equilibration the phonons carry the vast majority of energy density. Thus they dominate the reading of our thermometer. In order to compare the calculated lattice temperature to the measured strain at short timescales, we must include a modeling of the strain waves launched in the heterostructure, which are considerably driven by the electronic stress. Therefore, the spatio-temporal electron and phonon temperature maps in Figure 2 are used as input to calculate the transient strain by integrating a one dimensional masses-and-springs model.[36] It takes into account the absence of in-plane strains and the concomitant out-of-plane contraction.[37] The spatio-temporal strain $\eta(z, t)$ (**Figure 3**) is used to calculate the X-ray diffraction pattern by dynamical X-ray diffraction theory.[26,30,38]

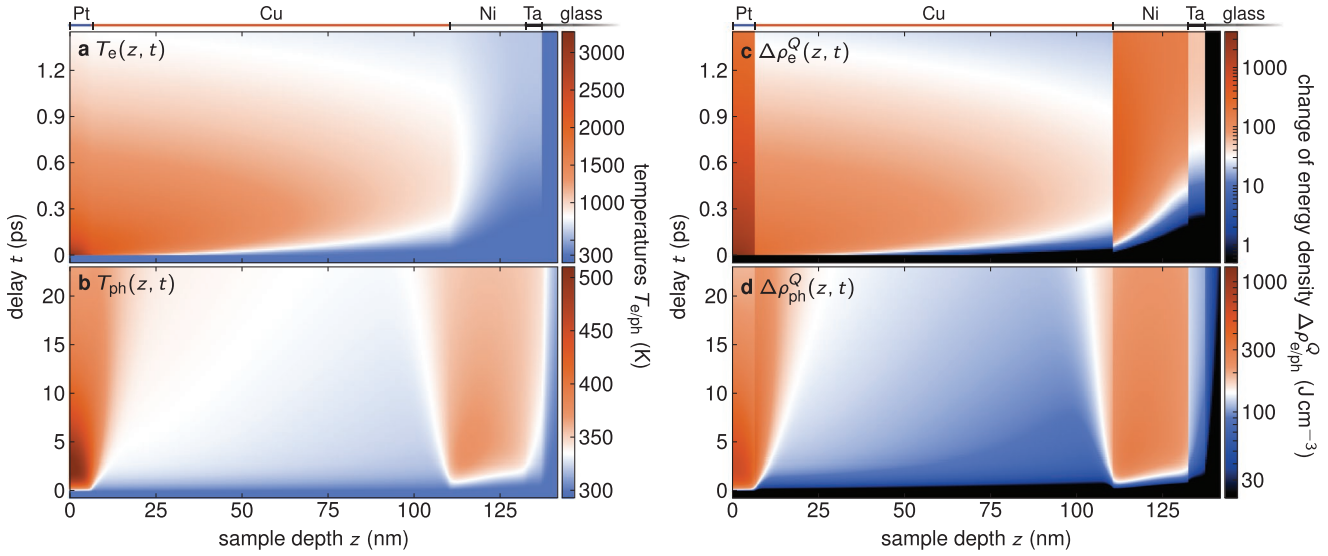

Figure 2. Result of the diffusive TTM of heat transport with temperature-dependent electron heat conductivity: a) Electron temperature, b) phonon temperature, c) change of electron energy density, and d) change of phonon energy density of the hetero-structure after excitation with an incident fluence of 20 mJ cm^{-2}. In the buried Ni film the energy density of the electron system and the lattice temperature rise faster than in the heat-conducting Cu layer.

The evaluation of the simulated Bragg peak shifts is plotted as continuous lines in **Figures** 1 and **4**.

Figure 4 compares two limiting cases calculated in the TTM to the continuous lines reproduced from Figure 1. The calculations leading to the dotted lines depict the dynamics that follow an instantaneously thermalized electron system that adopts a spatially homogeneous electron temperature throughout the heterostructure. This mimics the fastest possible electron transport that one would expect for approximate ballistic motion. We note, however, that homogeneous heating of the electron system necessarily would require also efficient scattering events within the Cu film. It strongly overestimates the expansion of the Ni layer and the relative amplitude of the Cu compression. As an opposite limit of slow transport, the modeling that yields the dashed lines assumes a temperature-independent electron heat conductivity. This leads to slower heat transport exaggerating the expansion of the Pt layer and underrating the Ni expansion, since the e-ph coupling dumps the energy to the Pt and Cu lattice before propagation to Ni. In this case also the initial compression of Cu is too short-lived because it now exclusively results from the Pt expansion.

We emphasize that only the TTM with temperature-dependent electron heat conductivity (continuous lines) can model the fluence dependence shown in Figure 1 with a fixed set of parameters. Figure 4d–f shows the simulated fluence dependence for the strain in all three layers normalized by the excitation fluence. The increased relative energy transport can be identified by the disproportionally increasing strain of the

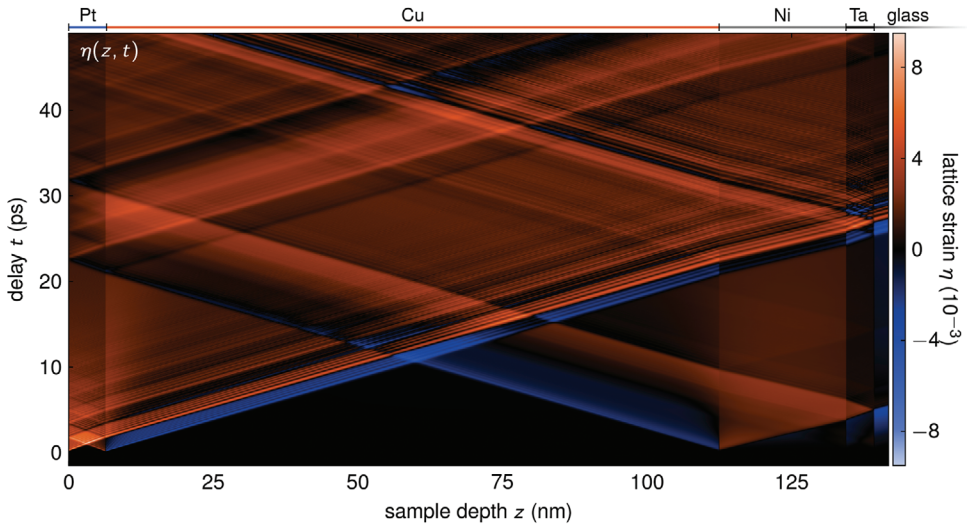

Figure 3. Calculated spatio-temporal strain $\eta(z, t)$ for an incidence fluence of 20 mJ cm^{-2}. After the excitation, the lattice starts to expand at the interfaces sending strain waves through the heterostructure. As indicated by the blue color, the Pt and Ni layers compress the Cu layer directly after excitation.

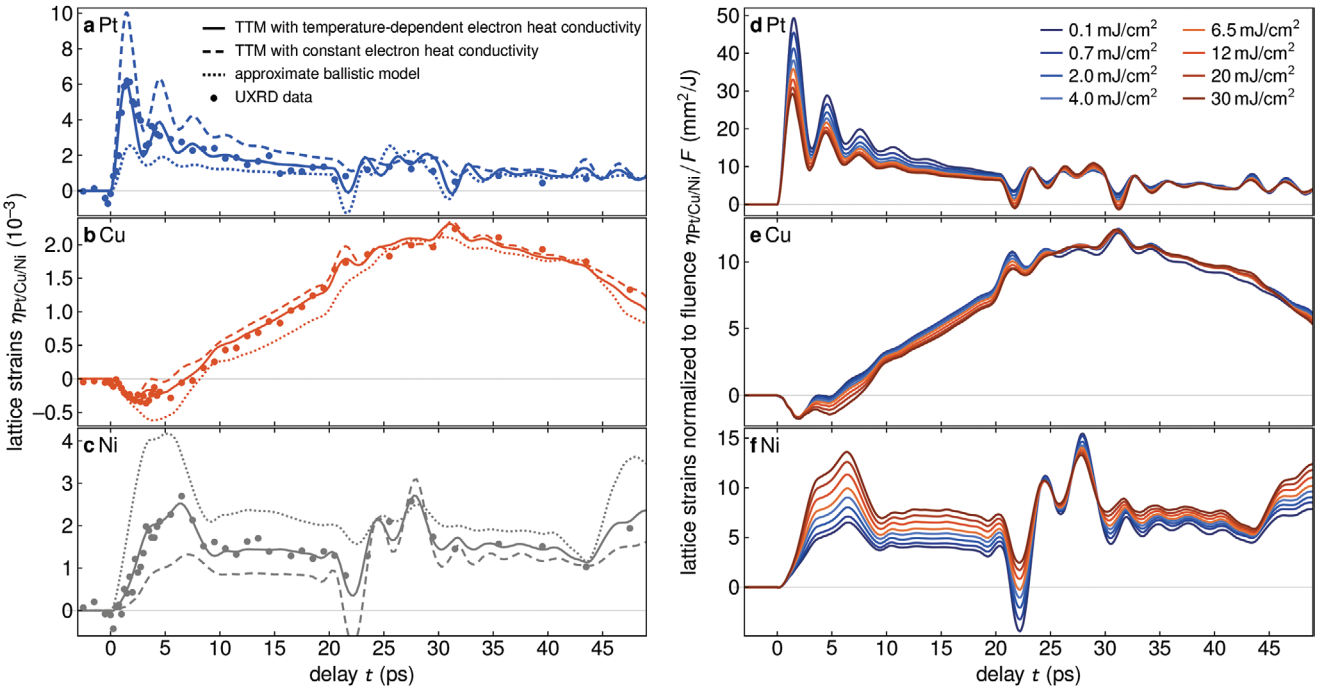

Figure 4. Limiting cases of electron transport and fluence dependence: Simulations of the UXRD data in comparison with the 20 mJ cm^{-2} UXRD data for a) Pt, b) Cu and c) Ni. The continuous lines originate from a simulation considering the temperature-dependent electron heat conductivity according to Equation (2). The dashed lines assume a constant electron heat conductivity with $T_e = T_{ph}$ in Equation (2) and the dotted lines result from an approximate ballistic model, which assumes a homogeneous initial electron temperature throughout the metal layers. The simulated fluence dependence with temperature-dependent electron heat conductivity reveals characteristic features: The strain of d) Pt and e) Cu normalized to the excitation fluence decreases with increasing fluence, whereas it increases for f) Ni. This is a manifestation of the enhanced thermal conductivities at elevated electron temperatures.

Ni layer with increased excitation fluence. The heat capacity of conduction electrons increases with temperature. Hence, for a temperature-independent e-ph coupling constant, the relaxation time in Pt is shorter at low fluence. This drives the high-frequency coherent oscillations originating in Pt more efficiently. Accordingly, at 22 ps the leading compression of the bipolar strain pulse originating from Pt strongly compresses the Ni layer. Normalized to the deposited energy, this compression is larger at low fluence. At high fluence, the increased electron heat conductivity in Cu (Equation (2)) and in parts also the longer e-ph coupling time in Pt facilitate a more efficient energy transport toward Ni. This causes the enhanced initial expansion of the Ni layer.

4. Discussion

Our diffusive model predicts that on a time scale of several tens of picoseconds heat is transported from Ni into the Cu lattice, that is, in the opposite direction of the initial heat flow in the electron system. This can be clearly seen in the temperature map at the Cu/Ni interface in Figure 2c. The inclusion of ballistic and superdiffusive aspects would even increase the electronic transport out of Pt through Cu into Ni and therefore enhance this backward heat transport.

In this article we do not take the challenge to fully model superdiffusive transport in this heterostructure, which would require a precise description of the band structures and all possible scattering processes of electrons and phonons of each material. Modeling the role of the interfaces would add yet another level of complexity. The mean free path $\xi \approx 25$ nm of electrons excited in Cu by 800 nm photons is considerably shorter than in noble metals,[39,40] making diffusive transport a reasonable approximation for 100 nm films. Therefore, we compare the diffusive to the ballistic limit in a simple manner. **Figure 5**a shows the normalized electron and lattice temperature evolution in Ni for different Cu layer thicknesses according to our fully diffusive model with temperature-dependent electron heat conductivity.

In order to illustrate that certain evaluations of experimental signatures may lead to erroneous conclusions regarding the mechanism of heat transport, we show different evaluations of the rise time of the Ni electron temperature in the first 6 ps in Figure 5b. The blue lines indicate the time at which the electronic temperature rises by selected absolute values ΔT_e^{Ni}. They show the expected depth dependence $z \propto \sqrt{t}$ for diffusive transport. Note that, for example, for $d \gtrsim 400$ nm the 10 K threshold in Ni is not overcome on the time scale of non-equilibrium electron conduction according to Equation (2). Instead, Ni is heated up by 10 K much later at about 1.5 ns (c.f. Figure 5a) via transport of locally equilibrated electrons and phonons. In contrast, the orange lines in Figure 5b report the time it takes the electron temperature in Nickel to rise to $f = 1\%$, $f = 10\%$ and $f = 33\%$ of the maximum electronic temperature in Ni

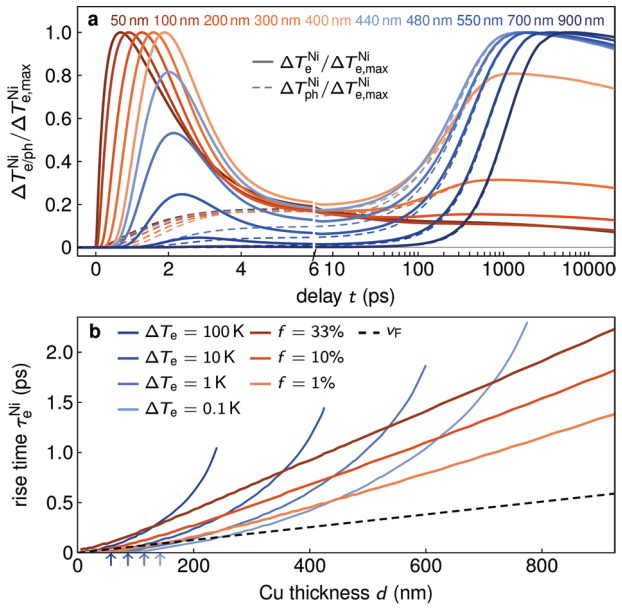

Figure 5. Dependence of the temperature evolutions in Ni on the thicknesses of the Cu transport layer. a) Transient layer-averaged electron and phonon temperature in Ni normalized to the respective maximum electron temperature for various thicknesses of the Cu layer. Up to approx. 400 nm the maximum temperature is reached within 2 ps by non-equilibrium heat transport according to Equation (5). Beyond this thickness near-equilibrium transport yields the maximum in the ns range. b) Rise time of the electron temperature in Ni to various absolute temperature thresholds ΔT_e^{Ni} in blue color code, together with arrows indicating up to which depth T_e^{Cu} has reached this threshold immediately by direct absorption of photons. Red color code for the rise time to various fractions f of maximum electron temperature, f. The time-length relation is linear for the relative threshold, whereas the absolute threshold yields the expected quadratic behavior.

within the first 6 ps for the respective Cu thickness. This rise to a certain percentage of the maximum is analogous to normalizing transients to their respective maximum and inferring the time-thickness relation by reading the crossing time for a given threshold f as reported in many studies.[12,41–43] This approach was first presented in the seminal paper by Brorson et al. on Au films[44] which are much thicker than the Cu films in similar early experiments.[45] The linear time-thickness relations found in those studies were interpreted as a manifestation of ballistic electron transport. Despite the purely diffusive character of our model, the analysis considering the rise time to a relative threshold f (orange lines in Figure 5b) also yields a linear dependence $z \propto t$ which is therefore obviously not a sufficient observation to conclude ballistic electron transport.[46] For comparison, the black dashed line in Figure 5b depicts the arrival time of ballistic electrons with Fermi velocity $v_F = 1.57 \times 10^6$ m s^{-1}[28] at the backside of a Cu layer of thickness d. For very thin Cu films and small relative temperature thresholds the diffusion appears to be faster than the ballistic motion. This is partially caused by the slight direct optical excitation of the Cu layer (see experimental section and arrows in Figure 5b). However, generally the diffusion approximation may yield heat transport that is faster than the group velocity of the heat carrying particles, that is, inconsistent with underlying concepts of the specific heat and heat transport by quasiparticles. Several approaches can be taken to cure this property of the heat equation,[3,10,47] which occurs when the length scale of the system is below the mean free path of the heat-carrying particles. The blue arrows in Figure 5b indicate, however, that the direct heating of Cu in a depth of 100 nm by the absorption of photons cannot be neglected when discussing tiny temperature changes (see figure caption for further details).

In the following, we investigate the origin of the surprising linear time-thickness relation from a fully diffusive model in more detail. For that purpose, we derive an analytic expression for electronic heat diffusion in the presence of e-ph coupling by solving the diffusive TTM (Equation (1)) for an isolated semi-infinite surface-heated Cu layer. For simplicity, we assume a constant phonon temperature $T_{ph} = T_e^0$, approximating $C_{ph} \gg C_e$, and a temperature-independent electron heat conductivity κ_e. This results in an uncoupled heat equation with a term accounting for the loss of heat from electrons to phonons:

$$\frac{\partial \Delta T_e}{\partial t} = \frac{\kappa_e}{C_e}\frac{\partial^2 \Delta T_e}{\partial z^2} - \frac{g}{C_e}\Delta T_e \tag{3}$$

with $\Delta T_e = T_e - T_{ph}$. The solution is given by

$$\Delta T_e(z,t) \propto \sqrt{\frac{C_e}{4\pi\kappa_e t}}\exp\left(-\frac{C_e z^2}{4\kappa_e t}\right)\exp\left(-\frac{g}{C_e}t\right) \tag{4}$$

which is a product of the Gaussian textbook solution of the heat equation and an exponential damping term due to e-ph coupling. At a distance $z = d$ from the heated surface, the electron temperature attains its maximum at time

$$t_{max} = \frac{C_e}{4g}\left(\sqrt{1+\frac{4g}{\kappa_e}d^2} - 1\right) \tag{5}$$

This expression is asymptotically linear for thick Cu layers with thickness $d \gg \sqrt{\kappa_e/4g} \approx 40$ nm which is consistent with our numerical solutions presented in Figure 5. The e-ph coupling strength g is crucial for the existence and timing t_{max} of the maximum electron temperature, and hence for the linear asymptotic dependence of Equation (5). We note that the numerical modeling including a temperature-dependent electron heat conductivity according to Equation (2) yields the same asymptotically linear behavior.

In summary, we emphasize the relevance of the non-equilibrium heat transport at small lengths scales as illustrated in Figure 5a: The normalized transient electron temperature rise in Ni is the decisive parameter, since it is the large electron heat capacity of Ni together with the large e-ph coupling in Ni which dominates the counter-intuitive phenomena. For thin Cu transport layers the maximum electron temperature in Ni is reached within the first 2 ps. For $d \gtrsim 400$ nm, the electron temperature has its maximum three orders of magnitude later, as the transport now occurs dominantly close to thermal equilibrium (cf. Figure 5a).

5. Conclusion

In conclusion, we presented ultrafast X-ray diffraction experiments that unveil unconventional heat transport by hot

electrons in a metallic heterostructure. After laser-heating the front end of the structure, the lattice of the back end is heated much more rapidly and efficiently than the part through which the heat is transported via conduction electrons. We highlight the crucial role of the high density of states at the Fermi level of the Ni layer at the back end of the structure. It attracts the heat energy ultrarapidly into its large heat reservoir and dumps the energy into lattice vibrations of Ni owing to its strong e-ph interaction. Subsequently, the lattice of the intermediate Cu layer is even heated from the backside. Our modeling approach considering purely diffusive transport reproduces our data very consistently, although partially ballistic or superdiffusive heat transport definitely occurs in Cu. The conceptual simplicity of our approach, however, also brings to light that the mere existence of a linear space-time relationship in the experimental data is not sufficient to identify a ballistic transport mechanism.

6. Experimental Section

Sample Growth: The metal heterostructure (Figure 1a) was sputtered onto a glass substrate (Corning 1737 AMLCD) in the following layering sequence: 6.6 nm Pt on 104 nm Cu on a 22 nm Ni on a 5 nm amorphous Ta adhesion layer. As described below, static X-ray diffraction reveals a (1 1 1)-orientation of the relaxed Pt, Cu and Ni layers.

UXRD Measurement: A reciprocal space map of the multilayer sample is obtained by detecting the symmetrically and asymmetrically diffracted X-rays on an area detector (Dectris PILATUS 100K) while sample and detector are rotated in a classical $\theta - 2\theta$ scheme. The reciprocal space map shows three material specific (1 1 1)-oriented Bragg peaks, which are located at $\theta_{Pt} = 19.75°$, $\theta_{Cu} = 21.65°$, and $\theta_{Ni} = 22.25°$. The sample was excited with *p*-polarized 100 fs laser pulses at 800 nm having an incident laser power of 330 mW or 110 mW at 1 kHz repetition rate. The footprint of laser beam was approximately 1.1×0.9 mm^2 (major and minor FWHM-diameter). For the 330 mW measurement the incidence angle of the laser was 50° (47.5°) with respect to the surface normal for the measurements on the Pt (Cu and Ni) Bragg reflection(s), which results in an incident fluence of 19 (20) mJ cm^{-2}. For the 110 mW measurement the incidence angle was 47.5° resulting in an incident fluence of 6.5 mJ cm^{-2}. The optical absorption profile calculated from the respective dielectric functions by a matrix formalism[25,48] reveals that over 86% of the absorbed energy of the near-infrared pump (800 nm) deposited inside the Pt layer and 14% are deposited in the first 12 nm ($1/e$) of the Cu layer. The sample was probed under a fixed angle with 200 fs X-ray probe pulses at a wavelength of 1.54 Å(Cu K_α) derived from the laser-driven plasma X-ray source (PXS)[49] and detected by an area detector at a fixed position. For each layer, the strain derived from the transient shift $\Delta\theta$ of the Bragg peak (center of mass) was used as a proportional measure of the average energy density in each layer.[25,26,50]

Simulation Methods: The TTM, strain, and X-ray diffraction simulations are carried out using the udkm1Dsim MATLAB toolbox.[30] For each material, values for the heat conductivities $\kappa_{e,ph}$, the specific heats $C_{e,ph}$, the Sommerfeld constants γ^S, and the electron-phonon coupling constants g are taken from the literature as given in Table 1. Constant values were applied for the specific heat and heat conductivity of the phonon system. Also the e-ph coupling parameter g was assumed to be temperature-independent, which is a reasonable approximation in the temperature range of the study. The electronic specific heat $C_e(T_e) = \gamma^S T_e$ depends on temperature according to the Sommerfeld model, and the temperature dependence of the non-equilibrium electron heat conductivity is given in Equation (2). The laser excitation is accounted for by the source term $S_e(z, t)$ whose spatial profile is dictated by the optical absorption calculated by a matrix formalism.[25,48] The calculated spatio-temporal electron and phonon temperature maps (Figure 2) were used as input to calculate the transient strain by integrating a linear masses-and-springs model[36] considering the geometrical limitation of thin films on ultrafast timescales.[27,37] The modeled strain was leveled to the 330 mW UXRD data by scaling the source term accordingly. The Grüneisen coefficient of Pt and Cu had to be adjusted by approximately ±20% to match the observed expansion between 300 ps to 1 ns, where the temperatures of all metal layers are in equilibrium. This is reasonable given that properties in thin films often slighlty differ from to bulk properties. All values are kept fixed for both fluences, that is, for the simulation matching the 110 mW UXRD data only the source term is divided by the factor 3. From the resulting strain map $\eta(z,t)$ (Figure 3), the X-ray diffraction pattern was calculated by dynamical X-ray diffraction theory. The calculated time-dependent Bragg peaks were evaluated in the same way as the experimental UXRD data to obtain the simulated transient layer-averaged strains shown in Figures 1 and 4.

Acknowledgements

The authors acknowledge the BMBF for the financial support via 05K16IPA and the DFG via BA 2281/8-1 and BA 2281/11-1. This work was supported partly by the French PIA project "Lorraine Université d'Excellence", reference ANR-15-IDEX-04-LUE, by the Project Plus cofounder by the "FEDER-FSE Lorraine et Massif Vosges 2014–2020", a European Union Program and by the OVNI projet from Region Grand and by the MATELAS projet institut Carnot ICEEL. The authors thank Felix Stete for providing the rendered sample illustration in Figure 1a. Open access funding enabled and organized by Projekt DEAL.

Conflict of Interest

The authors declare no conflict of interest.

Keywords

nanoscale heat transfer, thermal transport, ultrafast magnetism, ultrafast X-ray

Received: May 27, 2020
Revised: July 8, 2020
Published online: September 9, 2020

[1] D. G. Cahill, W. K. Ford, K. E. Goodson, G. D. Mahan, A. Majumdar, H. J. Maris, R. Merlin, S. R. Phillpot, *J. Appl. Phys.* **2003**, *93*, 793.
[2] D. G. Cahill, P. V. Braun, G. Chen, D. R. Clarke, S. Fan, K. E. Goodson, P. Keblinski, W. P. King, G. D. Mahan, A. Majumdar, H. J. Maris, S. R. Phillpot, E. Pop, L. Shi, *Appl. Phys. Rev.* **2014**, *1*, 011305.
[3] W. Dreyer, H. Struchtrup, *Continuum Mech. Thermodyn.* **1993**, *5*, 3.
[4] S. Weber, B. Rethfeld, *Appl. Surf. Sci.* **2017**, *417*, 64, 10th International Conference on Photoexcited Processes and Applications.
[5] P. Maldonado, K. Carva, M. Flammer, P. M. Oppeneer, *Phys. Rev. B* **2017**, *96*, 173.
[6] U. Ritzmann, P. M. Oppeneer, P. Maldonado, Theory of out-of-equilibrium electron and phonon dynamics in metals after ultrafast laser excitation, **2019**, URL http://arxiv.org/pdf/1911.12414v1.
[7] P. Maldonado, T. Chase, A. H. Reid, X. Shen, R. K. Li, K. Carva, T. Payer, M. Horn von Hoegen, K. Sokolowski-Tinten, X. J. Wang, P. M. Oppeneer, H. A. Dürr, *Phys. Rev. B* **2020**, *101*, 10.
[8] L. Waldecker, R. Bertoni, R. Ernstorfer, J. Vorberger, *Phys. Rev. X* **2016**, *6*, 945.
[9] M. Battiato, K. Carva, P. M. Oppeneer, *Phys. Rev. Lett.* **2010**, *105*, 027203.

[10] G. Chen, *Phys. Rev. Lett.* **2001**, *86*, 2297.
[11] M. Battiato, K. Carva, P. M. Oppeneer, *Phys. Rev. B* **2012**, *86*, 2.
[12] Y. Xu, M. Deb, G. Malinowski, M. Hehn, W. Zhao, S. Mangin, *Adv. Mater.* **2017**, *29*, 42.
[13] M. Deb, E. Popova, M. Hehn, N. Keller, S. Mangin, G. Malinowski, *Phys. Rev. B* **2018**, *98*, 444.
[14] A. V. Scherbakov, A. S. Salasyuk, A. V. Akimov, X. Liu, M. Bombeck, C. Brüggemann, D. R. Yakovlev, V. F. Sapega, J. K. Furdyna, M. Bayer, *Phys. Rev. Lett.* **2010**, *105*, 117204.
[15] J.-W. Kim, M. Vomir, J.-Y. Bigot, *Phys. Rev. Lett.* **2012**, *109*, 166601.
[16] O. Kovalenko, T. Pezeril, V. V. Temnov, *Phys. Rev. Lett.* **2013**, *110*, 266602.
[17] G. Malinowski, F. Dalla Longa, J. H. H. Rietjens, P. V. Paluskar, R. Huijink, H. J. M. Swagten, B. Koopmans, *Nat. Phys.* **2008**, *4*, 855.
[18] A. J. Schellekens, K. C. Kuiper, R. R. J. C. de Wit, B. Koopmans, *Nat. Commun.* **2014**, *5*, 4333.
[19] A. Melnikov, I. Razdolski, T. O. Wehling, E. T. Papaioannou, V. Roddatis, P. Fumagalli, O. Aktsipetrov, A. I. Lichtenstein, U. Bovensiepen, *Phys. Rev. Lett.* **2011**, *107*, 076601.
[20] Y. Yang, R. B. Wilson, J. Gorchon, C.-H. Lambert, S. Salahuddin, J. Bokor, *Sci. Adv.* **2017**, *3*, e1603117.
[21] R. B. Wilson, J. Gorchon, Y. Yang, C.-H. Lambert, S. Salahuddin, J. Bokor, *Phys. Rev. B* **2017**, *95*, 18.
[22] A. von Reppert, J. Pudell, A. Koc, M. Reinhardt, W. Leitenberger, K. Dumesnil, F. Zamponi, M. Bargheer, *Struct. Dyn.* **2016**, *3*, 054302.
[23] A. von Reppert, R. M. Sarhan, F. Stete, J. Pudell, N. Del Fatti, A. Crut, J. Koetz, F. Liebig, C. Prietzel, M. Bargheer, *J. Phys. Chem. C* **2016**, *120*, 28894.
[24] A. Koc, M. Reinhardt, A. von Reppert, M. Rössle, W. Leitenberger, K. Dumesnil, P. Gaal, F. Zamponi, M. Bargheer, *Phys. Rev. B* **2017**, *96*, 429.
[25] J. Pudell, A. A. Maznev, M. Herzog, M. Kronseder, C. H. Back, G. Malinowski, A. von Reppert, M. Bargheer, *Nat. Commun.* **2018**, *9*, 3335.
[26] J. Pudell, A. von Reppert, D. Schick, F. Zamponi, M. Rössle, M. Herzog, H. Zabel, M. Bargheer, *Phys. Rev. B* **2019**, *99*, 094304.
[27] A. von Reppert, M. Mattern, J.-E. Pudell, S. P. Zeuschner, K. Dumesnil, M. Bargheer, *Struct. Dyn.* **2020**, *7*, 024303.
[28] N. W. Ashcroft, N. D. Mermin, *Solid State Physics*, repr edition, Brooks/Cole Thomson Learning, South Melbourne **2012**.
[29] D. Schick, M. Herzog, A. Bojahr, W. Leitenberger, A. Hertwig, R. Shayduk, M. Bargheer, *Struct. Dyn.* **2014**, *1*, 064501.
[30] D. Schick, A. Bojahr, M. Herzog, R. Shayduk, C. von Korff Schmising, M. Bargheer, *Comput. Phys. Commun.* **2014**, *185*, 651.
[31] S.-S. Wellershoff, J. Hohlfeld, J. Güdde, E. Matthias, *Appl. Phys. A: Mater. Sci. Process.* **1999**, *69*, S99.
[32] A. P. Kanavin, I. V. Smetanin, V. A. Isakov, Y. V. Afanasiev, B. N. Chichkov, B. Wellegehausen, S. Nolte, C. Momma, A. Tünnermann, *Phys. Rev. B: Condens. Matter Mater. Phys.* **1998**, *57*, 14698.
[33] J. Hohlfeld, S.-S. Wellershoff, J. Güdde, U. Conrad, V. Jähnke, E. Matthias, *Chem. Phys.* **2000**, *251*, 237.
[34] P. B. Corkum, F. Brunel, N. K. Sherman, T. Srinivasan-Rao, *Phys. Rev. Lett.* **1988**, *61*, 2886.
[35] A. Block, M. Liebel, R. Yu, M. Spector, Y. Sivan, F. J. García de Abajo, N. F. van Hulst, *Sci. Adv.* **2019**, *5*, eaav8965.
[36] M. Herzog, D. Schick, P. Gaal, R. Shayduk, C. Korff Schmising, M. Bargheer, *Appl. Phys. A* **2012**, *106*, 489.
[37] A. von Reppert, L. Willig, J.-E. Pudell, S. P. Zeuschner, G. Sellge, F. Ganss, O. Hellwig, J. A. Arregi, V. Uhlíř, A. Crut, M. Bargheer, *Sci. Adv.* **2020**, *6*, eaba1142.
[38] S. P. Zeuschner, T. Parpiiev, T. Pezeril, A. Hillion, K. Dumesnil, A. Anane, J. Pudell, L. Willig, M. Rössle, M. Herzog, A. von Reppert, M. Bargheer, *Struct. Dyn.* **2019**, *6*, 024302.
[39] C. A. Schmuttenmaer, M. Aeschlimann, H. E. Elsayed-Ali, R. J. D. Miller, D. A. Mantell, J. Cao, Y. Gao, *Phys. Rev. B* **1994**, *50*, 8957.
[40] J. Cao, Y. Gao, H. E. Elsayed-Ali, R. J. D. Miller, D. A. Mantell, *Phys. Rev. B: Condens. Matter Mater. Phys.* **1998**, *58*, 10948.
[41] N. Bergeard, M. Hehn, S. Mangin, G. Lengaigne, F. Montaigne, M. L. M. Lalieu, B. Koopmans, G. Malinowski, *Phys. Rev. Lett.* **2016**, *117*, 147203.
[42] G. Malinowski, N. Bergeard, M. Hehn, S. Mangin, *Z. Phys. B: Condens. Matter Quanta* **2018**, *91*, 3251.
[43] T. Juhasz, H. E. Elsayed-Ali, G. O. Smith, C. Suárez, W. E. Bron, *Phys. Rev. B: Condens. Matter Mater. Phys.* **1993**, *48*, 15488.
[44] S. D. Brorson, J. G. Fujimoto, E. P. Ippen, *Phys. Rev. Lett.* **1987**, *59*, 1962.
[45] H. E. Elsayed-Ali, T. B. Norris, M. A. Pessot, G. A. Mourou, *Phys. Rev. Lett.* **1987**, *58*, 1212.
[46] H. Jang, J. Kimling, D. G. Cahill, *Phys. Rev. B* **2020**, *101*, 6.
[47] C. Cattaneo, J. K. de Fériet, Académie des sciences, *Sur une forme de l'équation de la chaleur éliminant le paradoxe d'une propagation instantanée*, Comptes rendus hebdomadaires des séances de l'Académie des sciences. Gauthier-Villars, **1958**.
[48] A. Eschenlohr, M. Battiato, P. Maldonado, N. Pontius, T. Kachel, K. Holldack, R. Mitzner, A. Föhlisch, P. M. Oppeneer, C. Stamm, *Nat. Mater.* **2014**, *13*, 102.
[49] D. Schick, A. Bojahr, M. Herzog, C. von Korff Schmising, R. Shayduk, W. Leitenberger, P. Gaal, M. Bargheer, *Rev. Sci. Instrum.* **2012**, *83*, 025104.
[50] D. Schick, R. Shayduk, A. Bojahr, M. Herzog, C. von Korff Schmising, P. Gaal, M. Bargheer, *J. Appl. Crystallogr.* **2013**, *46*, 1372.
[51] V. Y. Bodryakov, A. N. Bashkatov, *Russ. Metall (Metally)* **2013**, *2013*, 671.
[52] R. Shayduk, V. Vonk, B. Arndt, D. Franz, J. Strempfer, S. Francoual, T. F. Keller, T. Spitzbart, A. Stierle, *Appl. Phys. Lett.* **2016**, *109*, 043107.
[53] Corning Incorporated, *Corning 1737 AMLCD Glass*, **2002**.
[54] M. J. Duggin, *J. Phys. D: Appl. Phys.* **1970**, *3*, L21.
[55] X. Zheng, D. Cahill, P. Krasnochtchekov, R. Averback, J. Zhao, *Acta Mater.* **2007**, *55*, 5177.
[56] Z. Lin, L. V. Zhigilei, V. Celli, *Phys. Rev. B* **2008**, *77*, 075133.
[57] R. E. Macfarlane, J. A. Rayne, C. K. Jones, *Phys. Lett.* **1965**, *18*, 91.
[58] S. M. Collard, R. B. McLellan, *Acta Metall. Mater.* **1992**, *40*, 699.
[59] F. A. A. Radwan, *World Congress on Engineering 2012. July 4–6, 2012. London, UK*. **2010**, 2189 1221.
[60] H. M. Ledbetter, E. R. Naimon, *J. Phys. Chem. Ref. Data* **1974**, *3*, 897.
[61] J. R. Neighbours, F. W. Bratten, C. S. Smith, *J. Appl. Phys.* **1952**, *23*, 389.
[62] R. S. Krishnan, R. Srinivasan, S. Devanarayanan, B. R. Pamplin, *Thermal Expansion of Crystals: International Series in The Science of The Solid State*, Elsevier Science, Burlington **1979**.